Quantitative Measurement of Brain Perfusion with Intravoxel Incoherent Motion MR Imaging[1]

Christian Federau, MD, Dipl Phys ETH
Philippe Maeder, MD
Kieran O'Brien, PhD
Patrick Browaeys, MD
Reto Meuli, MD, PhD
Patric Hagmann, MD, PhD

Purpose: To evaluate the sensitivity of the perfusion parameters derived from Intravoxel Incoherent Motion (IVIM) MR imaging to hypercapnia-induced vasodilatation and hyperoxygenation-induced vasoconstriction in the human brain.

Materials and Methods: This study was approved by the local ethics committee and informed consent was obtained from all participants. Images were acquired with a standard pulsed-gradient spin-echo sequence (Stejskal-Tanner) in a clinical 3-T system by using 16 *b* values ranging from 0 to 900 sec/mm^2. Seven healthy volunteers were examined while they inhaled four different gas mixtures known to modify brain perfusion (pure oxygen, ambient air, 5% CO_2 in ambient air, and 8% CO_2 in ambient air). Diffusion coefficient (*D*), pseudodiffusion coefficient (*D**), perfusion fraction (*f*), and blood flow–related parameter (*fD**) maps were calculated on the basis of the IVIM biexponential model, and the parametric maps were compared among the four different gas mixtures. Paired, one-tailed Student *t* tests were performed to assess for statistically significant differences.

Results: Signal decay curves were biexponential in the brain parenchyma of all volunteers. When compared with inhaled ambient air, the IVIM perfusion parameters *D**, *f*, and *fD** increased as the concentration of inhaled CO_2 was increased (for the entire brain, $P = .01$ for *f*, *D**, and *fD** for CO_2 5%; $P = .02$ for *f*, and $P = .01$ for *D** and *fD** for CO_2 8%), and a trend toward a reduction was observed when participants inhaled pure oxygen (although $P > .05$). *D* remained globally stable.

Conclusion: The IVIM perfusion parameters were reactive to hyperoxygenation-induced vasoconstriction and hypercapnia-induced vasodilatation. Accordingly, IVIM imaging was found to be a valid and promising method to quantify brain perfusion in humans.

[1]From the Department of Diagnostic and Interventional Radiology, CHUV, University Hospital Center and University of Lausanne (CHUV-UNIL), Rue du Bugnon 46, 1011 Lausanne, Switzerland (C.F., P.M., P.B., R.M., P.H.); and CIBM, University of Geneva, Geneva, Switzerland (K.O.). Received March 10, 2012; revision requested May 8; revision received May 24; accepted June 6; final version accepted June 18. Supported in part by the Center for Biomedical Imaging of the Geneva and Lausanne Universities, EPFL. P.H. supported by Leenaards Foundation, Swiss National Science Foundation and Department of Radiology of University of Lausanne. **Address correspondence to** C.F. (e-mail: *christian.federau@chuv.ch*).

Perfusion is the process of nutritive delivery of arterial blood to the capillary bed of a biologic tissue (1). In the brain, it is classically quantified in terms of cerebral blood flow as a volume of blood per unit of the weight of the brain per unit of time (2). A variety of methods exist to measure brain perfusion by using magnetic resonance (MR) imaging. The most common method in clinical use, dynamic susceptibility contrast material–enhanced imaging, is based on the measurement of the first-pass T2* effect of a bolus of paramagnetic exogenous contrast material (gadolinium chelate) (3) and its volume distribution. A second method that is gaining popularity in recent years because of technical improvements is arterial spin labeling (4). It uses water in the blood as an endogenous contrast agent, which is labeled in the arteries before it enters the brain. A third method is dynamic contrast-enhanced MR imaging, which requires intravenous injection of gadolinium contrast media and measures the dynamic change in T1 relaxation time.

In all three techniques, perfusion quantification is dependent on the arterial input function, which is difficult to estimate because of bolus dispersion and delay (5–7). Furthermore, quantification requires many variables that induce additive effects on the error of the perfusion measure. Nonlinear signal changes are often ignored. Finally, dynamic contrast-enhanced MR imaging and dynamic susceptibility contrast-enhanced imaging are affected by first-pass extravasation of contrast material (8).

A fourth method, which is much less popular, called intravoxel incoherent motion (IVIM) imaging, measures perfusion locally and quantitatively (9). IVIM was introduced by Le Bihan et al (10) as a joint method to measure perfusion and diffusion. Although diffusion imaging has proved to be largely useful in a wide variety of clinical applications (11–14) as well as in more advanced applications such as diffusion tensor imaging and tractography (15–17), the measurement of perfusion by using IVIM is not common because of its low signal-to-noise ratio (18), with blood volume in the brain estimated to be in the low single-digit percentage range (19,20).

Recently, promising perfusion measurements with IVIM have been achieved in humans in multiple organs (21–28). However, to our knowledge, the last attempt to use the technique to measure perfusion in the brain was in the 1990s and was performed mostly in animals (29–31) and sporadically in humans (32–35). More recently, IVIM has been used in association with blood oxygenation level–dependent (36) and arterial spin labeling (37) techniques. A specific study validating the method in humans is, to our knowledge, lacking. Therefore, the purpose of this study was to evaluate the sensitivity of the perfusion parameters derived from Intravoxel Incoherent Motion (IVIM) in the human brain and MR imaging to hypercapnia-induced vasodilatation and hyperoxygenation-induced vasoconstriction.

Advances in Knowledge

- Imaging brain perfusion in humans with a clinical MR imaging unit is possible with intravoxel incoherent motion (IVIM) imaging.
- When compared with air inhalation, the IVIM perfusion parameters (pseudodiffusion coefficient, the perfusion fraction, and the flow-related parameter) increase gradually with inhalation of increasing CO_2 concentration (5% and 8% CO_2) ($P < .05$), which is known to vasodilate brain capillaries, and decrease under inhalation of pure O_2 ($P > .05$), which is known for its vasoconstrictive effect.

Implication for Patient Care

- Measurement of the highly clinically relevant cerebral blood flow with IVIM has many theoretical advantages over currently available perfusion imaging methods because it is noninvasive and nonirradiating, requires no intravenous contrast material injection, is probably mainly dependent on capillary flow (little arterial or venous sensitivity), and is intrinsically quantitative.

Materials and Methods

This prospective study was approved by the local ethics committee at the University of Lausanne. Informed consent was obtained from all participants. Imaging was performed in seven healthy volunteers (five men, two women; mean age, 28) who were more than 18 years old from September through November 2011. No volunteers were excluded during this study. Imaging was performed by two radiologists (C.F. and P.H., with 1 year and 7 years of experience in radiology, respectively). Image processing and analysis and statistical analysis were done by C.F. Results analysis and text writing was performed by all authors.

IVIM Model

The IVIM model can be understood as an adaptation of Stejskal's and Tanner's work (38) on biologic tissue, and was proposed by Le Bihan et al (10,34). The hypothesis is that two compartments exist: a slow moving compartment, where particles diffuse in a Brownian fashion as a consequence of thermal energy, and a fast moving compartment (the vascular compartment), where blood moves

Published online before print
10.1148/radiol.12120584 **Content code:** NR

Radiology 2012; 265:874–881

Abbreviations:
D = diffusion coefficient
*D** = pseudodiffusion coefficient
f = perfusion fraction
*fD** = flow-related parameter
IVIM = intravoxel incoherent motion

Author contributions:
Guarantors of integrity of entire study, C.F., P.M., R.M., P.H.; study concepts/study design or data acquisition or data analysis/interpretation, all authors; manuscript drafting or manuscript revision for important intellectual content, all authors; approval of final version of submitted manuscript, all authors; literature research, C.F., P.M., K.O., R.M., P.H.; clinical studies, C.F., P.B., R.M., P.H.; experimental studies, C.F., P.M., P.H.; statistical analysis, C.F., P.H.; and manuscript editing, C.F., P.M., K.O., P.B., P.H.

Conflicts of interest are listed at the end of this article.

as a consequence of pressure gradient. In this second compartment, a pseudodiffusion term (D^*) is introduced that describes on a macroscopic level the displacement of the blood elements in an assumed randomly laid vascular network. For the perfusion to have a physiologic meaning, one expects that D^* is greater than D. Therefore:

$$\frac{S(b)}{S_0} = fe^{-bD^*} + (1-f)e^{-bD} \quad (1)$$

where f is the perfusion fraction; D, the diffusion coefficient; D^*, the pseudodiffusion coefficient; and:

$$b = \gamma^2 G^2 \delta^2 (\Delta - \frac{\delta}{3}) \quad (2)$$

The b value regroups the parameters depending on the sequence, namely the gyromagnetic ratio (γ), and the duration (δ), strength (G), and interval (Δ) of the magnetic field gradient.

Imaging Parameters

Data were acquired by using a 3-T MR imager (Trio; Siemens, Erlangen, Germany) with a 32-channel receiver head coil and a standard monopolar pulsed-gradient spin-echo echo-planar imaging sequence (33,38), which is used routinely for diffusion-weighted imaging. For each participant, we acquired images of nine axial brain sections with the following paramenters: section thickness, 4 mm; field of view, 297 × 297 mm^2; matrix, 256 × 256, in-plane resolution, 1.2 × 1.2 mm^2; repetition time/echo time, 4000/99 msec; parallel imaging with an acceleration factor of two; and 75% partial Fourier encoding. Receiver bandwidth was 1086 Hz/pixel. Fat was suppressed with a frequency-selective saturation routine. We acquired images at multiple b values (0, 10, 20, 40, 80, 110, 140, 170, 200, 300, 400, 500, 600, 700, 800, and 900 sec/mm^2) in three orthogonal directions, averaged four times. Total acquisition time was 12 minutes and 28 seconds.

Gas Inhalation

Increase in CO_2 arterial partial pressure is a well-known potent intracerebral vasodilator that increases cerebral blood flow; inhalation of pure oxygen has been shown to significantly decrease cerebral blood flow (39). We investigated in two healthy volunteers (one man and one woman, mean age, 26 years) the variation of the IVIM parameters in the brain after inhalation of ambient air (22% O_2, 78% N_2), and a mixture of 5% CO_2 and air (5% CO_2, 22% O_2, 73% N_2), and in five healthy volunteers (four men and one woman; mean age, 28 years) after inhalation of ambient air, a mixture of 5% CO_2 and ambient air, and 8% CO_2 and ambient air (8% CO_2, 22% O_2, 70% N_2), and pure oxygen (100% O_2). One experiment was interrupted during the 8% CO_2 inhalation because of technical problems (participant 3 in Table 1). The gases were kept in bottles outside the Faraday cage, and were provided to the volunteers through an airtight mask over the nose and mouth and a one-way valve system. We waited a fixed time of 6 minutes for equilibrium between gas switches and acquisitions. For safety reasons, expiratory partial pressure of CO_2 was monitored by using a Maglife C Plus monitor (Schiller Medical, Wissembourg, France) or capillary partial pressure of CO_2 was monitored transcutaneously with a TOSCA 500 monitor (Radiometer, Thalwil, Switzerland) (40).

Image Processing

Geometric distortion and bulk motion correction were removed with the FSL (*http://www.fmrib.ox.ac.uk/fsl/index.html*) eddy-current image registration tool before the IVIM calculation (41). All images were registered to the image with a b value of 0. Curve fitting of equation 1 was done on a voxel-by-voxel basis by using the Levenberg-Marquardt algorithm (42) implemented with standard Matlab functions (Mathworks, Natick, Massachusetts). In the first step, the curve was fitted for a b value greater than 200 sec/mm^2 for the single parameter, D. The assumption for this step was that D^* is significantly greater than D, so that the influence of D^* on signal decay can be neglected for b factors greater than 200 sec/mm^2 (43). In the second step, the curve was fitted for f and D^* for all the b values, while keeping D constant. This two-step method was found to be more robust than a direct biexponential fit. For example, in the case of a voxel with a monoexponential signal decay, a direct biexponential fit would weight the first or second exponential in an aleatory way, giving meaningless values for f. Values less than 0 for f, D, and D^* are not physiologic and were set to 0, as were values greater than 1 for f. Values with f greater than 0.3 and D^* greater than 0.05 were set (arbitrarily) to zero because they are not physiologic and likely to result either from noise or turbulent cerebrospinal fluid flow.

Image Analysis

A whole brain region of interest (ROI) was first drawn on images of each axial section, and the IVIM parameters were calculated on a voxel-by-voxel basis and averaged (more than 100 000 voxels in each participant). Furthermore, we placed small ROIs (approximately 1–2 cm^2) on images of the gray matter of the superior frontal and parietal gyri, in the white matter of the center semiovale, in the thalamus, and the lenticular nucleus on both sides. The fit was done again on a voxel-by-voxel basis and the result was averaged for each small ROI and then averaged for the gray matter, white matter, thalamus and lenticular nucleus. IVIM parameter maps were generated to demonstrate the voxel-by-voxel percentage variations under the various gases in comparison to those under ambient air.

Statistical Analysis

Normal data distribution was assumed and not tested owing to the low number of data. A paired one-tailed Student t test was performed by using Excel (Microsoft, Redmont, Wash) to reject the null hypothesis that the results obtained under hypercapnia and hyperoxygenation were similar to those obtained with ambient air. A P value less than .05 was considered to indicate a statistically significant difference. Multiple testing analysis was not performed.

Results

In all seven volunteers, the signal decay curve as function of b, with b ranging

Table 1

IVIM Perfusion Parameters on Inhalation of Four Gases Averaged in Whole Brain Parenchyma

Volunteer	Gas	*f* (%)	*D** (10^{-3} mm^2 · sec^{-1})	*fD** (10^{-3} mm^2 · sec^{-1})	*D* (10^{-3} mm^2 · sec^{-1})
1	Air	5.55 ± 8.66	6.17 ± 10.06	0.45 ± 0.96	0.82 ± 0.80
	5% CO_2	5.85 ± 8.80	7.07 ± 10.88	0.52 ± 1.04	0.81 ± 0.80
2	Air	5.92 ± 8.88	6.66 ± 10.38	0.48 ± 0.94	0.80 ± 0.86
	5% CO_2	6.60 ± 9.00	7.90 ± 11.16	0.58 ± 1.04	0.79 ± 0.84
3	O_2	5.87 ± 8.28	6.86 ± 10.14	0.59 ± 1.14	0.99 ± 0.96
	Air	6.27 ± 8.26	7.08 ± 9.82	0.58 ± 1.00	0.96 ± 0.94
	5% CO_2	6.56 ± 8.26	7.57 ± 10.26	0.62 ± 1.02	0.96 ± 0.94
4	O_2	5.69 ± 6.54	7.30 ± 10.08	0.56 ± 1.00	0.91 ± 0.88
	Air	5.91 ± 7.60	7.96 ± 10.66	0.61 ± 1.04	0.91 ± 0.88
	5% CO_2	5.98 ± 7.66	7.75 ± 10.42	0.60 ± 1.04	0.91 ± 0.86
	8% CO_2	6.13 ± 7.88	8.73 ± 11.18	0.71 ± 1.18	0.90 ± 0.86
5	O_2	6.16 ± 8.08	7.49 ± 10.16	0.60 ± 1.00	0.94 ± 0.86
	Air	6.29 ± 8.04	7.28 ± 9.76	0.58 ± 0.94	0.93 ± 0.86
	5% CO_2	6.29 ± 7.94	7.49 ± 10.42	0.59 ± 0.98	0.93 ± 0.84
	8% CO_2	7.31 ± 8.70	9.70 ± 12.40	0.87 ± 1.34	0.97 ± 0.82
6	O_2	6.49 ± 7.62	8.18 ± 10.08	0.66 ± 1.02	0.94 ± 0.80
	Air	6.23 ± 7.44	8.37 ± 10.42	0.64 ± 1.00	0.93 ± 0.80
	5% CO_2	6.58 ± 7.84	8.76 ± 10.72	0.69 ± 1.04	0.90 ± 0.76
	8% CO_2	7.33 ± 7.80	10.74 ± 12.80	0.91 ± 1.30	0.88 ± 0.74
7	O_2	5.92 ± 8.02	6.22 ± 9.12	0.53 ± 1.06	0.94 ± 0.90
	Air	6.23 ± 8.04	6.48 ± 9.50	0.58 ± 1.16	0.96 ± 0.90
	5% CO_2	6.74 ± 9.22	7.66 ± 10.72	0.69 ± 1.38	0.98 ± 0.92
	8% CO_2	6.68 ± 8.80	7.64 ± 10.80	0.74 ± 1.48	0.92 ± 0.88

Note.—Data are means ± standard deviation, obtained by averaging the values obtained pixel by pixel throughout the entire acquired brain.

from 0 to 900 sec/mm^2, was biexponential (ie, two straight lines could be seen in logarithmic scale independently of the size of the ROI).

In the ROI of the entire brain, *f*, *D**, and *fD** showed a statistically significant increase ($P = .01$ for *f*, *D**, and *fD** for 5% CO_2; $P = .02$ for *f*, and $P = .01$ for *D** and *fD** for 8% CO_2) with CO_2 inhalation compared with air (Tables 1, 2; Fig 1), and larger mean values when the percentage of CO_2 was incrementally increased from 5% to 8% ($P = .08$ for *f*; $P = .04$ for *D**; $P = .02$ for *fD**). We also observed a trend toward a reduction of the IVIM perfusion parameters when the patient inhaled pure O_2 compared with air ($P = .11$ for *f*; $P = .09$ for *D**; $P = .38$ for *fD**).

The results obtained in the small ROIs were similar to those obtained for the entire brain (Fig 2), but with a higher variance than for the whole-brain results. When compared with air inhalation, differences were mostly statistically significant ($P < .05$, Fig 2) for CO_2 inhalation at various concentrations and showed a trend for O_2.

The effects of hypercapnia and hyperoxygenation were essentially restricted to *b* values less than 200 sec/mm^2, although a small effect for *b* values greater than 200 sec/mm^2 (*D* seems to be slightly reduced with 8% CO_2), cannot be excluded from this study (Fig 2d).

Surprisingly, under hypercapnia, *f* decreased in the cerebrospinal fluid in the sulci (Fig 3). This corresponded to a decrease of turbulent flow in the cerebrospinal fluid, which we assumed was due to an increase in brain volume in the constant skull volume and a consecutive decrease in cerebrospinal fluid volume. This phenomenon was also observed recently during functional MR imaging experiments (44,45).

Discussion

The results of this study validate IVIM imaging as a method to measure perfusion in the human brain. To our knowledge, this was not previously well established in the literature. Our results demonstrated that *f*, *D**, and *fD** change in a gradual way under hypercapnia and hyperoxygenation stimuli in the full brain and in smaller ROIs. It is an important step in confirming the feasibility of IVIM imaging as a quantitative method to measure brain perfusion.

The measurement of IVIM perfusion parameters in the full brain seems to be robust in this small cohort, with an intersubject standard deviation of approximately 10% of the mean for *f*, *D**, and *fD**, which is similar to the standard deviation obtained for *D*. Although the graded response indicates sensitivity to cerebral perfusion, the high intrasubject standard deviations,

Figure 1

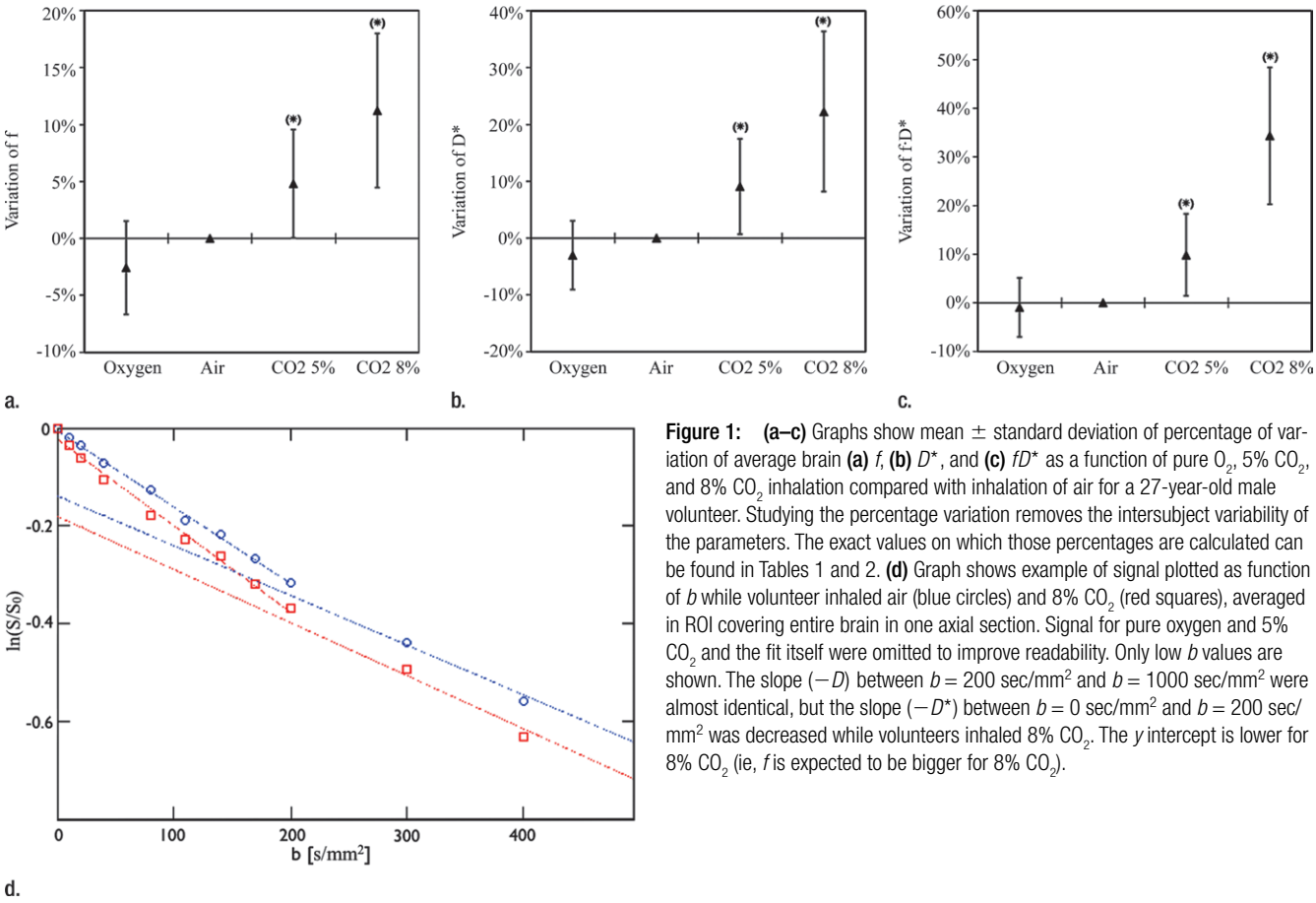

Figure 1: **(a–c)** Graphs show mean ± standard deviation of percentage of variation of average brain **(a)** *f*, **(b)** *D**, and **(c)** *fD** as a function of pure O_2, 5% CO_2, and 8% CO_2 inhalation compared with inhalation of air for a 27-year-old male volunteer. Studying the percentage variation removes the intersubject variability of the parameters. The exact values on which those percentages are calculated can be found in Tables 1 and 2. **(d)** Graph shows example of signal plotted as function of *b* while volunteer inhaled air (blue circles) and 8% CO_2 (red squares), averaged in ROI covering entire brain in one axial section. Signal for pure oxygen and 5% CO_2 and the fit itself were omitted to improve readability. Only low *b* values are shown. The slope ($-D$) between $b = 200$ sec/mm^2 and $b = 1000$ sec/mm^2 were almost identical, but the slope ($-D^*$) between $b = 0$ sec/mm^2 and $b = 200$ sec/mm^2 was decreased while volunteers inhaled 8% CO_2. The *y* intercept is lower for 8% CO_2 (ie, *f* is expected to be bigger for 8% CO_2).

Table 2

IVIM Perfusion Parameters in Full Brain with Inhalation of Four Different Gases

No. of Volunteers	Gas	*f* [%]	*P* Value	D* (10^{-3} mm^2 · s^{-1})	*P* Value	*fD** (10^{-3} mm^2 · s^{-1})	*P* Value	*D* (10^{-3} mm^2 · s^{-1})
4	O_2	6.02 ± 0.31	.11	7.21 ± 0.72	.09	0.59 ± 0.04	.38	0.95 ± 0.02
7	Air	6.05 ± 0.27	. . .	7.14 ± 0.74	. . .	0.57 ± 0.06	. . .	0.90 ± 0.06
7	5% CO_2	6.37 ± 0.34	.01	7.74 ± 0.68	.01	0.61 ± 0.06	.01	0.90 ± 0.08
6	8% CO_2	6.86 ± 0.57	.02	9.20 ± 0.94	.01	0.80 ± 0.10	.01	0.90 ± 0.02

Note.—Data are means ± standard deviation, as obtained by averaging the results presented in Table 1. *P* values were calculated in comparison with ambient air.

which were of more than 100% of the mean, could be due to the limited precision of the method, but could also be explained by the physiologic heterogeneity of the brain.

Interestingly, in the smaller ROIs in various brain regions, the variability increases significantly for *f*, *D**, and *fD**, but not for *D*, in comparison with the full-brain results. This could be due to low signal-to-noise ratio, slight motion during the acquisition, partial volume effects with cerebrospinal fluid, or could reflect true physiologic variability. Large variations in vascular response to hypercapnia between and within participants, both in amplitude and in spatial distribution (which may not be simply attributed to measurement errors) were observed in several studies (46–50). Spatially heterogeneous response and highly variable changes (with standard deviations more than 100% of the means) in the diameters of capillaries and velocities of red blood cells were found in rats by using two-photon microscopy (46). Regional differences in

Radiology

Figure 2

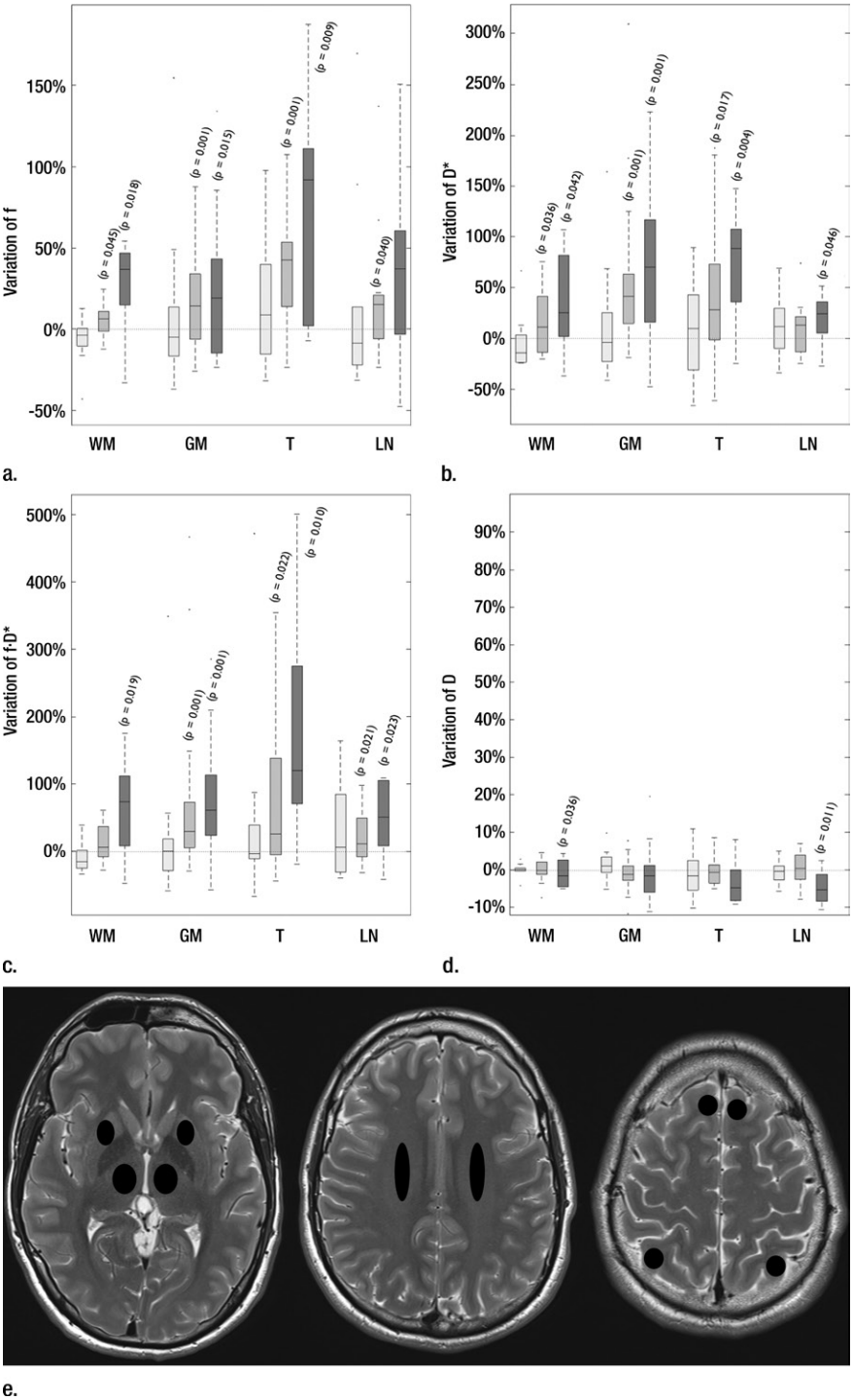

Figure 2: Box and whisker plots (median, 25th and 75th percentiles, minimum, maximum, outliers) compare variations of **(a)** *f*, **(b)** *D**, **(c)** *fD**, and **(d)** *D*, averaged in ROIs drawn in white matter *(WM)*, gray matter *(GM)*, thalamus *(T)*, and lenticular nucleus *(LN)*, in four to seven volunteers and in both sides of the brain. White = percent changes of pure oxygen compared with air, light gray = percent changes of 5% CO_2 compared with air, dark gray = percent changes of 8% CO_2 compared with air. *P* values compared with air are indicated when statistically significant. **(e)** Axial T2-weighted MR images show ROIs drawn to avoid as much cerebrospinal fluid as possible.

vascular response to changes in arterial partial pressure of CO_2 have been reported in humans with positron emission tomography as well (47).

This study had some general limitations. The cohort of seven volunteers was small, and the study was performed at a single center. The order of the sequence of acquisitions was not randomized. The physiologic effect of hypercapnia and hyperoxygenation may have varied during image acquisitions. The intrasubject reproducibility was not studied. Partial volume effects with cerebrospinal fluid may have been variable during the experiment.

Nevertheless, quantification of cerebral blood perfusion with current methods, such as dynamic susceptibility contrast-enhanced and dynamic contrast-enhanced MR imaging and arterial spin labeling, remains a major challenge for many reasons (5–8). Therefore, despite its current limitations, perfusion measurement with IVIM, because it is intrinsically local and quantitative, deserves more attention (9) and further development.

Many technical limitations persist, and improvements could increase IVIM image quality. Although echo-planar techniques allow for fast imaging, the need for acquisitions with multiple *b* values extends acquisition time and makes the technique very motion-sensitive if the curve is fitted on a voxel-by-voxel basis. Furthermore, the important differences in contrast between the images acquired with different *b* values increase the difficulties for the postprocessing of motion corrections. Interactions between the different magnetic gradient fields, for example, between imaging gradients and Stejskal-Tanner gradients, could alter the effective *b* value, especially at a low *b* value. Beyond perfusion, the IVIM method is dependent on the capillary

Figure 3

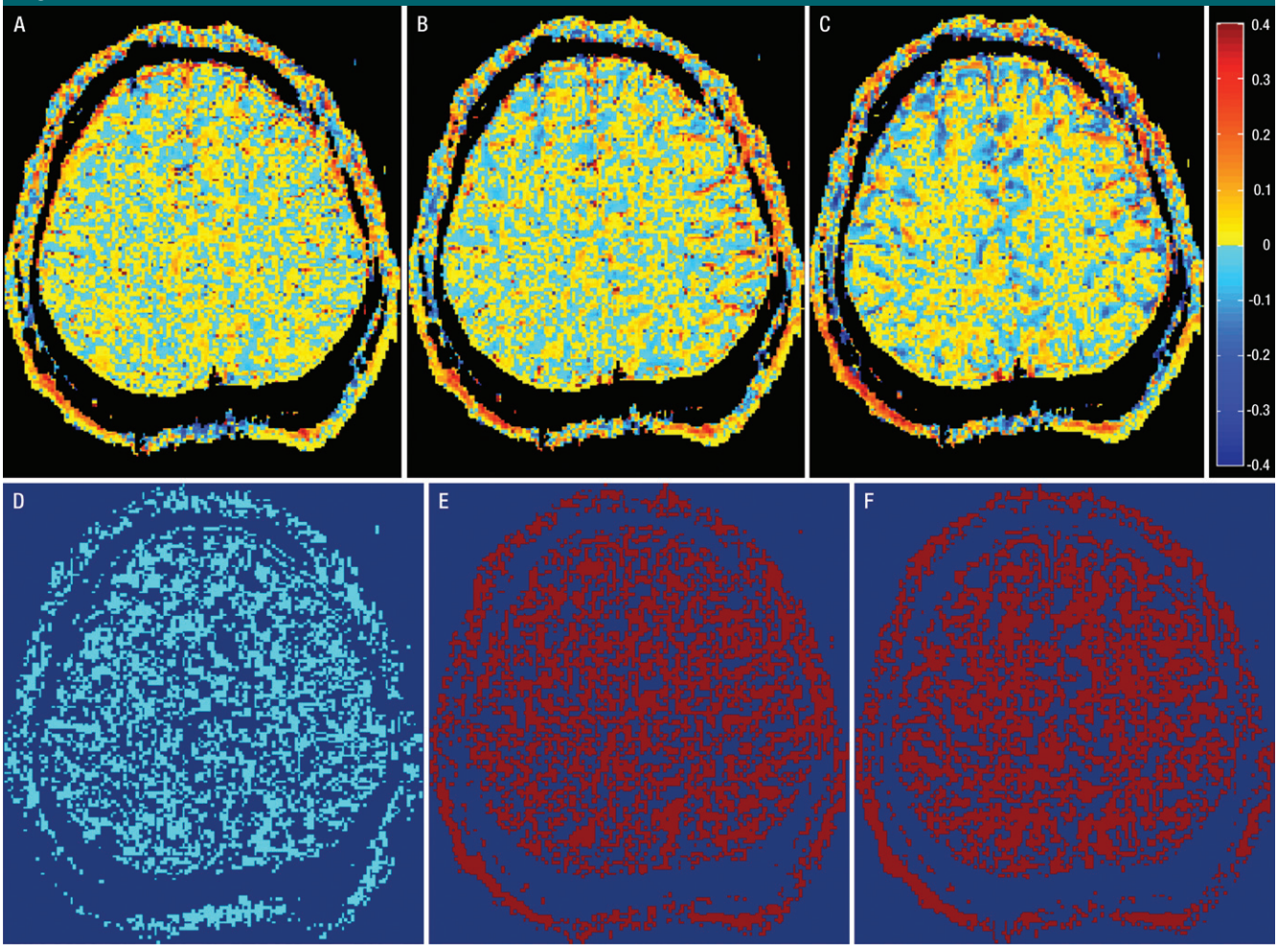

Figure 3: Pixelwise change in *f* obtained by subtracting the *f* map under, *A,* hyperoxygenation, *B,* 5% CO_2, and *C,* 8% CO_2 from the *f* map under ambient air. "Hot" colors (yellow to red) mean increase with respect to air; "cold" colors (light to dark blue) mean strict decrease. Note in *B* and *C* that increase in *f* is predominantly in cortex and that *f* in cerebrospinal fluid decreases. *D,* In light blue are pixels from *A* that strictly decrease under inhalation of pure O_2 compared with ambient air. *E, F,* In red are pixels that strictly increase under inhalation of, *E,* 5% and, *F,* 8% CO_2 in air compared with ambient air.

microarchitecture (51), a property that could prove useful, for example, in the study of tumor neoangiogenesis, where the capillary bed structure could differ significantly from the norm.

In conclusion, the results of this study show that IVIM can measure perfusion quantitatively in the human brain. Improvements in the certainty of parameter estimates should be pursued. Studies assessing the clinical applicability of the method are still lacking.

Acknowledgments: The authors thank the volunteers, as well as Markus Klarhoefer, Nicolas Croxatto, the MR technicians team of CHUV, especially Nicolas Chevrey and Boris Mrdovic, and Siemens, for providing us with the necessary modifications to the sequence.

Disclosures of Conflicts of Interest: C.F. Financial activities related to the present article: none to disclose. Financial activities not related to the present article: institution has patent pending related to IVIM. Other relationships: none to disclose. **P.M.** Financial activities related to the present article: none to disclose. Financial activities not related to the present article: institution has patent pending related to IVIM. Other relationships: none to disclose. **K.O.** No relevant conflicts of interest to disclose. **P.B.** No relevant conflicts of interest to disclose. **R.M.** No relevant conflicts of interest to disclose. **P.H.** Financial activities related to the present article: none to disclose. Financial activities not related to the present article: institution has patent pending related to IVIM. Other relationships: none to disclose.

References

1. Krogh A. The anatomy and physiology of capillaries. New Haven, Conn: Yale University Press, 1922.
2. Kety SS, Schmidt CF. The nitrous oxide method for the quantitative determination of cerebral blood flow in man: theory, procedure and normal values. J Clin Invest 1948;27(4):476–483.
3. Villringer A, Rosen BR, Belliveau JW, et al. Dynamic imaging with lanthanide chelates in normal brain: contrast due to magnetic susceptibility effects. Magn Reson Med 1988; 6(2):164–174.
4. Dixon WT, Du LN, Faul DD, Gado M, Rossnick S. Projection angiograms of blood la-

beled by adiabatic fast passage. Magn Reson Med 1986;3(3):454–462.

5. Calamante F, Gadian DG, Connelly A. Quantification of perfusion using bolus tracking magnetic resonance imaging in stroke: assumptions, limitations, and potential implications for clinical use. Stroke 2002;33(4):1146–1151.
6. Knutsson L, Ståhlberg F, Wirestam R. Absolute quantification of perfusion using dynamic susceptibility contrast MRI: pitfalls and possibilities. MAGMA 2010;23(1):1–21.
7. Petersen ET, Zimine I, Ho YC, Golay X. Non-invasive measurement of perfusion: a critical review of arterial spin labelling techniques. Br J Radiol 2006;79(944):688–701.
8. Paulson ES, Schmainda KM. Comparison of dynamic susceptibility-weighted contrast-enhanced MR methods: recommendations for measuring relative cerebral blood volume in brain tumors. Radiology 2008;249(2):601–613.
9. Le Bihan D. Intravoxel incoherent motion perfusion MR imaging: a wake-up call. Radiology 2008;249(3):748–752.
10. Le Bihan D, Breton E, Lallemand D, Grenier P, Cabanis E, Laval-Jeantet M. MR imaging of intravoxel incoherent motions: application to diffusion and perfusion in neurologic disorders. Radiology 1986;161(2):401–407.
11. Maier SE, Sun Y, Mulkern RV. Diffusion imaging of brain tumors. NMR Biomed 2010;23(7):849–864.
12. Mikulis DJ, Roberts TP. Neuro MR: protocols. J Magn Reson Imaging 2007;26(4):838–847.
13. Roberts TP, Mikulis D. Neuro MR: principles. J Magn Reson Imaging 2007;26(4):823–837.
14. Schellinger PD, Jansen O, Fiebach JB, et al. Feasibility and practicality of MR imaging of stroke in the management of hyperacute cerebral ischemia. AJNR Am J Neuroradiol 2000;21(7):1184–1189.
15. Hagmann P, Kurant M, Gigandet X, et al. Mapping human whole-brain structural networks with diffusion MRI. PLoS ONE 2007; 2(7):e597.
16. Yamada K, Sakai K, Akazawa K, Yuen S, Nishimura T. MR tractography: a review of its clinical applications. Magn Reson Med Sci 2009; 8(4):165–174.
17. Bammer R, Holdsworth SJ, Veldhuis WB, Skare ST. New methods in diffusion-weighted and diffusion tensor imaging. Magn Reson Imaging Clin N Am 2009;17(2):175–204.
18. Pekar J, Moonen CT, van Zijl PC. On the precision of diffusion/perfusion imaging by gradient sensitization. Magn Reson Med 1992; 23(1):122–129.
19. Ito H, Kanno I, Iida H, et al. Arterial fraction of cerebral blood volume in humans measured by positron emission tomography. Ann Nucl Med 2001;15(2):111–116.
20. Kim T, Kim SG. Quantification of cerebral arterial blood volume and cerebral blood flow using MRI with modulation of tissue and vessel (MOTIVE) signals. Magn Reson Med 2005; 54(2):333–342.
21. Koh DM, Collins DJ, Orton MR. Intravoxel incoherent motion in body diffusion-weighted MRI: reality and challenges. AJR Am J Roentgenol 2011;196(6):1351–1361.
22. Luciani A, Vignaud A, Cavet M, et al. Liver cirrhosis: intravoxel incoherent motion MR imaging—pilot study. Radiology 2008;249(3): 891–899.
23. Callot V, Bennett E, Decking UK, Balaban RS, Wen H. In vivo study of microcirculation in canine myocardium using the IVIM method. Magn Reson Med 2003;50(3):531–540.
24. Lemke A, Laun FB, Klauss M, et al. Differentiation of pancreas carcinoma from healthy pancreatic tissue using multiple b-values: comparison of apparent diffusion coefficient and intravoxel incoherent motion derived parameters. Invest Radiol 2009;44(12):769–775.
25. Sigmund EE, Cho GY, Kim S, et al. Intravoxel incoherent motion imaging of tumor microenvironment in locally advanced breast cancer. Magn Reson Med 2011;65(5):1437–1447.
26. Thoeny HC, Binser T, Roth B, Kessler TM, Vermathen P. Noninvasive assessment of acute ureteral obstruction with diffusion-weighted MR imaging: a prospective study. Radiology 2009;252(3):721–728.
27. Karampinos DC, King KF, Sutton BP, Georgiadis JG. Intravoxel partially coherent motion technique: characterization of the anisotropy of skeletal muscle microvasculature. J Magn Reson Imaging 2010;31(4):942–953.
28. Riches SF, Hawtin K, Charles-Edwards EM, de Souza NM. Diffusion-weighted imaging of the prostate and rectal wall: comparison of biexponential and monoexponential modelled diffusion and associated perfusion coefficients. NMR Biomed 2009;22(3):318–325.
29. Henkelman RM, Neil JJ, Xiang QS. A quantitative interpretation of IVIM measurements of vascular perfusion in the rat brain. Magn Reson Med 1994;32(4):464–469.
30. Le Bihan D, Moonen CT, van Zijl PC, Pekar J, DesPres D. Measuring random microscopic motion of water in tissues with MR imaging: a cat brain study. J Comput Assist Tomogr 1991;15(1):19–25.
31. Neil JJ, Bosch CS, Ackerman JJ. An evaluation of the sensitivity of the intravoxel incoherent motion (IVIM) method of blood flow measurement to changes in cerebral blood flow. Magn Reson Med 1994;32(1):60–65.
32. Chenevert TL, Pipe JG, Williams DM, Brunberg JA. Quantitative measurement of tissue perfusion and diffusion in vivo. Magn Reson Med 1991;17(1):197–212.
33. Turner R, Le Bihan D, Maier J, Vavrek R, Hedges LK, Pekar J. Echo-planar imaging of intravoxel incoherent motion. Radiology 1990;177(2):407–414.
34. Le Bihan D, Breton E, Lallemand D, Aubin ML, Vignaud J, Laval-Jeantet M. Separation of diffusion and perfusion in intravoxel incoherent motion MR imaging. Radiology 1988;168(2):497–505.
35. Wirestam R, Brockstedt S, Lindgren A, et al. The perfusion fraction in volunteers and in patients with ischaemic stroke. Acta Radiol 1997;38(6):961–964.
36. Song AW, Fichtenholtz H, Woldorff M. BOLD signal compartmentalization based on the apparent diffusion coefficient. Magn Reson Imaging 2002;20(7):521–525.
37. Kim T, Kim SG. Quantification of cerebral arterial blood volume using arterial spin labeling with intravoxel incoherent motion-sensitive gradients. Magn Reson Med 2006;55(5):1047–1057.
38. Stejskal EO, Tanner JE. Spin diffusion measurements: spin echoes in the presence of a time-dependent field gradient. J Chem Phys 1965;42(1):288–292.
39. Kety SS, Schmidt CF. The effects of altered arterial tensions of carbon dioxide and oxygen on cerebral blood flow and cerebral oxygen consumption of normal young men. J Clin Invest 1948;27(4):484–492.
40. Parker SM, Gibson GJ. Evaluation of a transcutaneous carbon dioxide monitor ("TOSCA") in adult patients in routine respiratory practice. Respir Med 2007;101(2):261–264.
41. Smith SM, Jenkinson M, Woolrich MW, et al. Advances in functional and structural MR image analysis and implementation as FSL. Neuroimage 2004;23(Suppl 1):S208–S219.
42. Seber GA, Wild CJ. Nonlinear regression. Hoboken, NJ: Wiley-Interscience, 2003.
43. Le Bihan D, Turner R, MacFall JR. Effects of intravoxel incoherent motions (IVIM) in steady-state free precession (SSFP) imaging: applicatons to molecular diffusion imaging. Magn Reson Med 1989;10(3):324–337.
44. Piechnik SK, Evans J, Bary LH, Wise RG, Jezzard P. Functional changes in CSF volume estimated using measurement of water T2 relaxation. Magn Reson Med 2009;61(3): 579–586.
45. Jin T, Kim SG. Change of the cerebrospinal fluid volume during brain activation investigated by T(1rho)-weighted fMRI. Neuroimage 2010;51(4):1378–1383.
46. Ho YC, Petersen ET, Zimine I, Golay X. Similarities and differences in arterial responses to hypercapnia and visual stimulation. J Cereb Blood Flow Metab 2011;31(2):560–571.
47. Hutchinson EB, Stefanovic B, Koretsky AP, Silva AC. Spatial flow-volume dissociation of the cerebral microcirculatory response to mild hypercapnia. Neuroimage 2006;32(2): 520–530.
48. Ito H, Kanno I, Fukuda H. Human cerebral circulation: positron emission tomography studies. Ann Nucl Med 2005;19(2):65–74.
49. Leontiev O, Buxton RB. Reproducibility of BOLD, perfusion, and CMRO2 measurements with calibrated-BOLD fMRI. Neuroimage 2007;35(1):175–184.
50. Piechnik SK, Chiarelli PA, Jezzard P. Modelling vascular reactivity to investigate the basis of the relationship between cerebral blood volume and flow under CO2 manipulation. Neuroimage 2008;39(1):107–118.
51. Le Bihan D, Turner R. The capillary network: a link between IVIM and classical perfusion. Magn Reson Med 1992;27(1):171–178.